The Fate of Primary Iron Sulfides in the Highly-altered CM1(/2) Carbonaceous Chondrites

S. A. Singerling[1], C. M. Corrigan[2], and A. J. Brearley[1]

[1]Department of Earth and Planetary Sciences, MSC03-2040, 1 University of New Mexico, Albuquerque, NM 87131.
[2]Department of Mineral Sciences, National Museum of Natural History, Smithsonian Institution, Washington, DC 20560-0119.
Email: ssingerling@unm.edu

Introduction

- Potential primary sulfides: pyrrhotite ($(Fe,Ni)_{1-x}S$, po) and pentlandite ($(Fe,Ni)_9S_8$, pn)
- Formation mechanisms:
  - **Crystallization:** cooling of sulfide melts produced during chondrule formation events [1-6]
    - Produced the pyrrhotite-pentlandite intergrowth (PPI) grains (Fig. 1a-c) [7]
  - **Sulfidization:** Fe,Ni-metal + H_2S = $(Fe,Ni)_{1-x}S$ [5, 8-10]
    - Produced the sulfide-rimmed metal (SRM) grains (Fig. 1d-f) [7]

Objectives: What are the effects and mechanisms of extensive alteration of primary pyrrhotite and pentlandite as observed in the CM1(/2) chondrites?

How do these compare to sulfides previously observed in CM1 chondrites [11]?

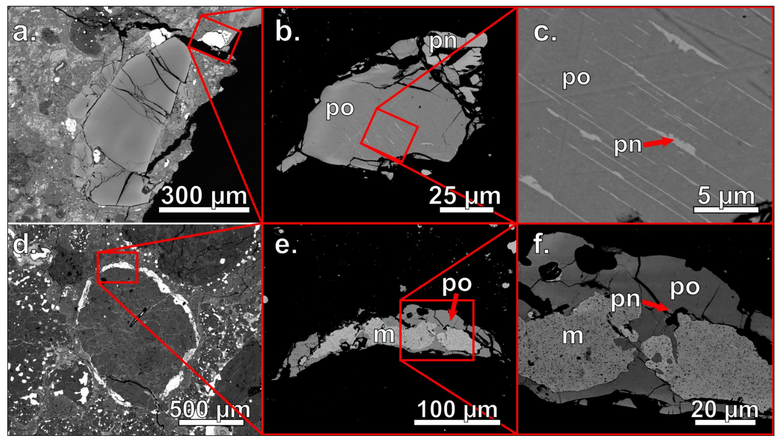

Fig. 1. BSE images, along with contextual information, of primary sulfides in CM2 and CR2 chondrites which formed by crystallization (a-c) and sulfidization (d-f). The top three images are from CM2 QUE 97990 and illustrate the features of the PPI grains, such as abundant po-pn exsolution textures (pn patches and lamellae). The bottom three images are from CR2 EET 92042 and illustrate the features of the SRM grains, such as a kamacite core rimmed by po with minor pn exsolution. po = pyrrhotite, pn = pentlandite, m =Fe,Ni metal.

Methods

- Meteorites studied: CM1/2s ALHA 83100, ALH 84029, 84034, 84049, LAP 031166, and CM1 MET 01073
- FEI Nova NanoSEM 600 (NMNH) = BSE images
- FEI Quanta 3D Dualbeam® FEGSEM/FIB (UNM) = FIB section preparation
- JEOL 8200 EPMA (Institute of Meteoritics, UNM) = WDS compositional data
- JEOL 2010F STEM (UNM) = EDS analyses/X-ray maps, HAADF images

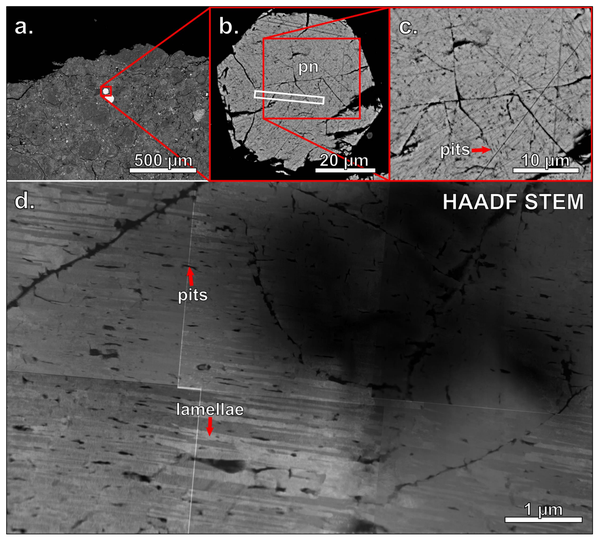

Fig. 2. BSE (a-c) and HAADF STEM (d) images of a 3P grain in ALH 84049. The white rectangle in (b) depicts the location where a FIB section was extracted. (d) presents a mosaic of the FIB section; the tiled appearance is an artifact of imaging. Note the crystallographically-oriented pits and the presence of lamellae/twinning only visible on the TEM scale. pn = pentlandite.

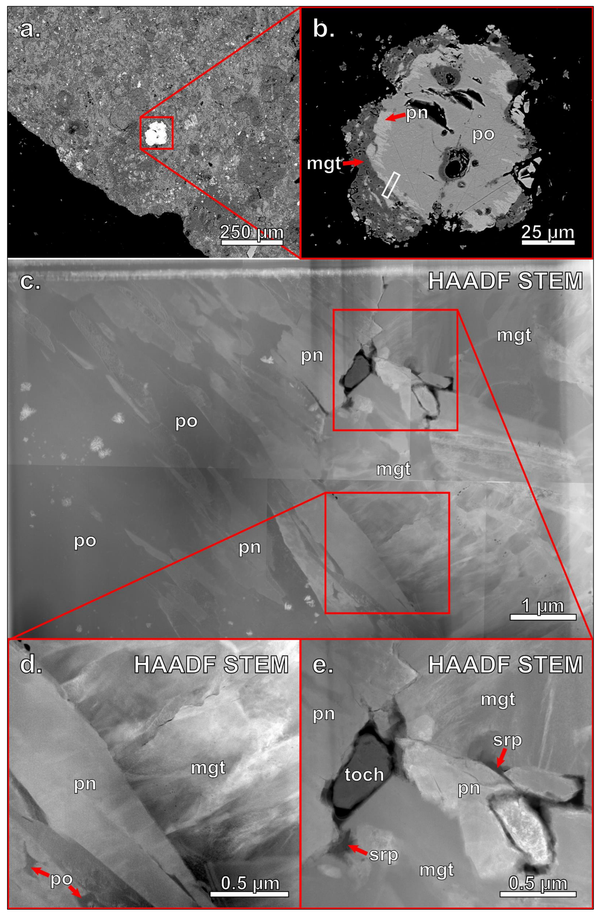

Fig. 3. BSE (a-b) and HAADF STEM (c-e) images of a PPM grain in ALHA 83100. The white rectangle in (b) depicts the location where a FIB section was extracted. (d) presents a mosaic of the FIB section; the tiled appearance is an artifact of imaging. Note the complex phase assemblage at the po-mgt boundary in (e). po= pyrrhotite, pn = pentlandite, mgt =magnetite, srp = serpentine, toch = tochilinite.

Results

Altered primary sulfide textural groups in the CM1(/2) chondrites:

1) Porous, Pitted Pentlandite (**3P**) grains (Fig. 2)
   - Located in CM chondrite matrix and relict chondrules
   - Grains of pn exhibiting porosity that appears crystallographically controlled (Fig. 2d)
   - CM2 precursor = 4P grains of [12]
2) Pyrrhotite+Pentlandite+Magnetite (**PPM**) grains (Fig. 3)
   - Located in CM chondrite matrix and relict chondrules
   - Primary phases = po + pn; secondary phases = magnetite (mgt) + pn ± serpentine (srp)
   - Also observed by [11]
3) Pentlandite+Serpentine (**PS**) grains (Fig. 4)
   - Located in CM chondrite matrix and relict chondrules
   - Primary phases = pn; secondary phases = srp + pn ± mgt
4) Pyrrhotite+Pentlandite+Magnetite+Serpentine (**PPMS**) grains (Fig. 5)
   - Located in CM chondrite matrix
   - Transitional between the PPM and PS grains
   - Primary phases = po + pn; secondary phases = mgt + pn + srp

Table 1. Textural groups, proportions, sizes, spatial occurrence, and exsolution textures of altered primary sulfide grains in the CM1(/2) chondrites studied

Sample	Textural Group	n	Size Range (µm)	Spatial Occurrence	Exsolution Textures
ALH 84029	3P	5	18-85	matrix	N/A
	PPM	4	30-110	matrix	p,b,r
	PS	3	30-40	chondrule, matrix	p,b
	PPMS	2	60-125	matrix	p,l
ALH 84034	3P	5	10-25	chondrule, matrix	N/A
	PPM	3	25-40	matrix	p
	PS	5	15-60	chondrule, matrix	p,b,l
ALH 84049	3P	3	55-75	matrix	N/A
	PPM	6	30-55	chondrule, matrix	p
	PS	4	35-130	chondrule, matrix	p,b
	PPMS	1	35	matrix	p
ALHA 83100	PPM	6	15-90	chondrule, matrix	p,b,r
LAP 031166	3P	1	35	matrix	N/A
	PS	1	25	matrix	p,r
	PPMS	1	65	matrix	p,r
MET 01073	3P	1	35	matrix	N/A
	PS	5	30-70	chondrule, matrix	p,b,r

* p = patches, b = blades, l = lamellae, r = rods, N/A = no textures were present

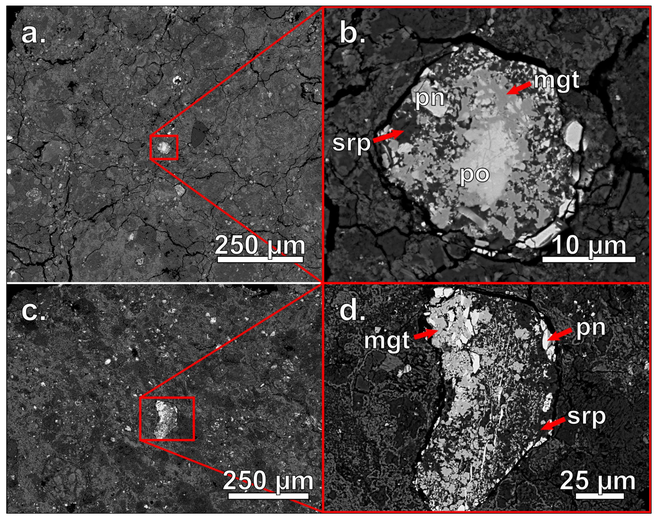

Fig. 5. BSE images, along with contextual information, of PPMS grains in CM1/2s (a-c) ALH 84049 and (d-f) ALH 84029. In both grains, pentlandite patches, surrounded by magnetite veining, are visible near the grain boundary. In the less-altered grain (b), pyrrhotite is present, and there is less magnetite, serpentine, and rod-form pentlandite. pn = pentlandite, mgt = magnetite, srp = serpentine.

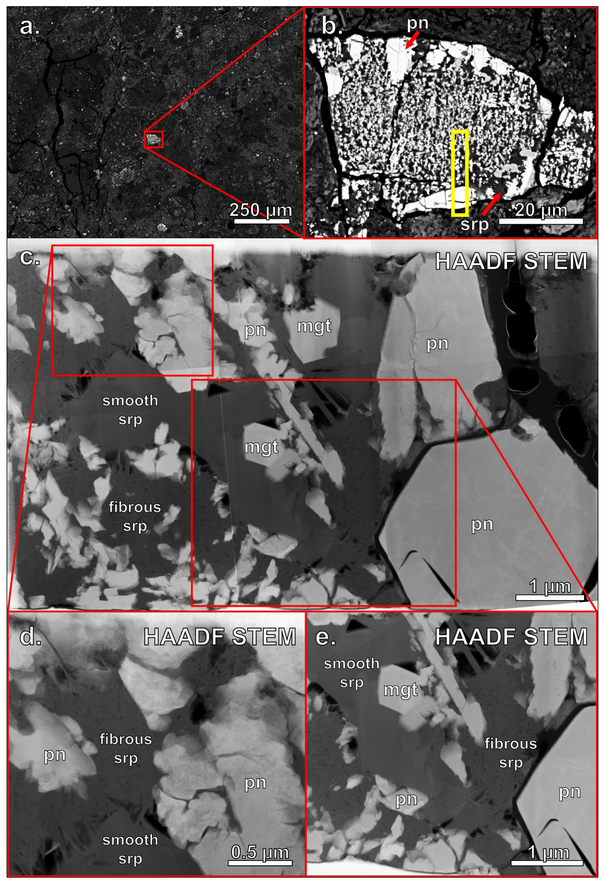

Fig. 4. BSE (a-b) and HAADF STEM (c-e) images of a PS grain in ALH 84049. The yellow rectangle in (b) depicts the location where a FIB section was extracted. (d) presents a mosaic of the FIB section; the tiled appearance is an artifact of imaging. Note the presence of both a smooth- and a fibrous-textured serpentine in (c-e). pn = pentlandite, mgt =magnetite, srp = serpentine

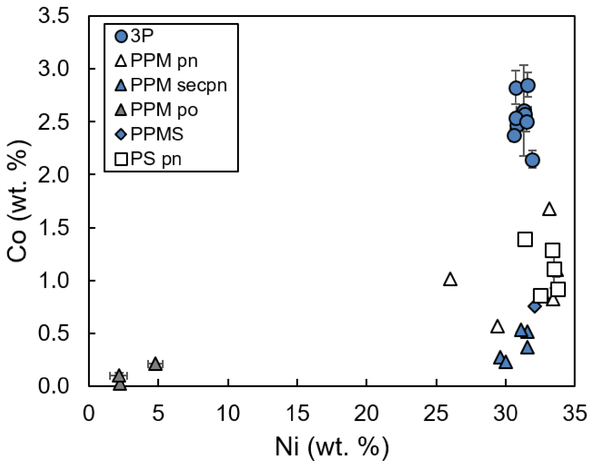

Fig. 6. Element-element plots (in wt.%) for CM1(/2) altered primary sulfides. Points are averages of individual EPMA point analyses for an individual phase within the grains. Error bars represent 1σ standard deviation. The points are differentiated by textural group. Three groups of pn are visible: 1) low-Co group consisting of secondary pn in PPM and PPMS grains, 2) moderate-Co group consisting of primary PPM and PS pn, and 3) high-Co group consisting of 3P pn. po = pyrrhotite, pn = pentlandite, sec = secondary.

Discussion: Formation Mechanisms

- Precursors to these altered grains were PPI grains
- **3P grains** = dissolution of po with replacement by secondary pn
  - Product of a more extensive degree of alteration that appears to continue from the degree seen in CM2 chondrites
  - Requires acidic conditions along with a Ni-bearing fluid

PPI to 3P reaction

$$\text{pyrrhotite} + Ni^{2+}(aq) \rightarrow \text{pentlandite} + S^{2-}(aq) + Fe^{2+}(aq)$$
$$(Fe,Ni)_{1-x}S(s) + Ni^{2+}(aq) \rightarrow (Fe,Ni)_9S_8(s) + S^{2-}(aq) + Fe^{2+}(aq)$$

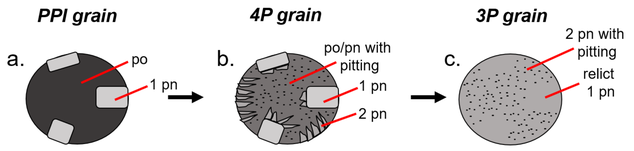

Fig. 7. Schematic representing progressive sequence of alteration of PPI grains to the 4P and 3P grains.
(a) PPI grain is stable prior to alteration having originally formed in the solar nebula from crystallization of sulfide melts during chondrule formation.
(b) Changes in environmental conditions (such as a decrease in pH) cause dissolution of pyrrhotite forming numerous submicron pits. The dissolution of pyrrhotite also causes remaining, adjacent pyrrhotite to transform into secondary pentlandite. Primary pyrrhotite is still present at this stage. 4P grains are a sample of the alteration to this point.
(c) Continued alteration causes all primary pyrrhotite to be replaced by secondary pentlandite. Only primary and secondary, pitted pentlandite (blue circles in Fig. 6) remain at this stage. 3P grains are a sample of the extensive alteration to this point. po = pyrrhotite, 1 pn = primary pentlandite, 2 pn = secondary pentlandite.

- **PPM/PS/PPMS grains** = oxidation by Ni-bearing fluid replaces po with mgt and secondary pn, changing fluid composition causes mgt to alter to serpentine
  - Strong link between these three grain types as evidenced by transitional PPMS grains, the presence of small amounts of srp in PPM grains (Fig. 3e), and the presence of relict mgt in PS grains (Fig. 4c, e)
  - Requires oxidizing conditions along with a Ni-bearing fluid followed by a Si,Mg-bearing fluid

PPI to PPM reaction

$$\text{pyrrhotite} + Ni^{2+}(aq) + O_2(aq) \rightarrow \text{magnetite} + \text{pentlandite} + S^{2-}(aq) + Fe^{2+}(aq)$$
$$(Fe,Ni)_{1-x}S(s) + Ni^{2+}(aq) + O_2(aq) \rightarrow Fe_3O_4(s) + (Fe,Ni)_9S_8(s) + S^{2-}(aq) + Fe^{2+}(aq)$$

PPM to PS reaction

$$\text{magnetite} + Si^{4+}(aq) + Mg^{2+}(aq) + O_2(aq) \rightarrow \text{serpentine}$$
$$Fe_3O_4(s) + 2Si^{4+}(aq) + 3Mg^{2+}(aq) + 2H_2O(l) \rightarrow (Fe,Mg)_3Si_2O_5(OH)_4(s)$$

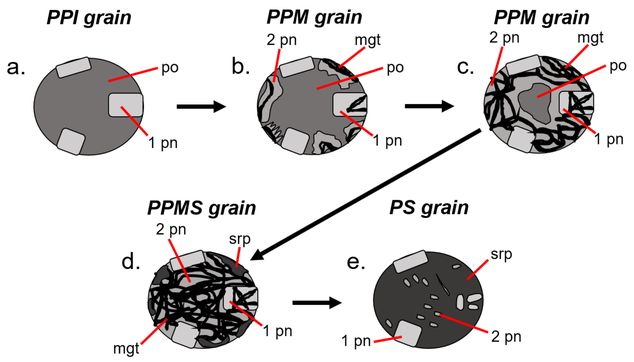

Fig. 8. Schematic representing progressive sequence of alteration of PPI grains to the PPM, PPMS, and PS grains.
(a) PPI grain is stable prior to alteration having originally formed in the solar nebula from crystallization of sulfide melts during chondrule formation.
(b) Changes in environmental conditions (fO_2) cause oxidation of pyrrhotite forming magnetite. Secondary pentlandite (blue triangles in Fig. 6) also forms during the replacement of pyrrhotite by magnetite. PPM grains are a sample of the alteration to this point.
(c) Continued alteration causes more primary pyrrhotite to be replaced by magnetite and secondary pentlandite (blue diamond in Fig. 6).
(d) Additional changes in environmental conditions (fluid composition) cause replacement of magnetite by serpentine. The primary and secondary pentlandite are resistant to alteration. PPMS grains are a sample of the alteration to this point.
(e) Continued alteration causes more magnetite to be replaced by serpentine until only primary (white squares in Fig. 6) and secondary pentlandite and serpentine remain. PS grains are a sample of the alteration to this point. po = pyrrhotite, 1 pn = primary pentlandite, 2 pn = secondary pentlandite, mgt =magnetite, srp = serpentine.

Conclusion

These altered primary sulfide grains clearly indicate the complex nature of the aqueous alteration environment with evidence for acidic and oxidizing conditions as well as changing fluid compositions.

Acknowledgements: This work was supported by NASA Cosmochemistry grant NNX11AK51G to AJ Brearley (PI).

References: [1] Boctor N. Z. et al. (2002) LPS XXXIII, Abstract #1534. [2] Brearley A. J. and Martinez C. (2010) LPS XLIII, Abstract #1438. [3] Maldonado E. M. and Brearley A. J. (2011) LPS XLII, Abstract #2271. [4] Harries D. and Langenhorst F. (2013) MAPS, 48, 879-903. [5] Schrader D. L. et al. (2015) MAPS, 50, 15-50. [6] Schrader D. L. et al. (2016) GCA, 189, 359-76. [7] Singerling S. A. and Brearley A. J. (2015) LPS XLVI, Abstract #1059. [8] Zanda B. et al. (1995) Meteoritics, 30, 605. [9] Lauretta D. S. et al. (1998) MAPS, 33, 821-33. [10] Schrader D. L. and Lauretta D. S. (2010) GCA 74, 1719-33. [11] Zolensky M. E. et al. (1997) GCA, 61, 5099-115. [12] Singerling S. A. and Brearley A. J. (2016) LPS XLVII, Abstract #1718.